ACS Biomaterials SCIENCE & ENGINEERING

Article

pubs.acs.org/journal/abseba

Transport of Nitric Oxide (NO) in Various Biomedical grade Polyurethanes: Measurements and Modeling Impact on NO Release Properties of Medical Devices

Hang Ren,[†] Joseph L. Bull,[‡] and Mark. E. Meyerhoff*[,†]

[†]Department of Chemistry, University of Michigan, 930 North University, Ann Arbor, Michigan 48109, United States

[‡]Department of Biomedical Engineering, University of Michigan, 2200 Bonisteel Boulevard, Ann Arbor, Michigan 48109, United States

Supporting Information

ABSTRACT: Nitric oxide (NO) releasing polymers are promising in improving the biocompatibility of medical devices. Polyurethanes are commonly used to prepare/fabricate many devices (e.g., catheters); however, the transport properties of NO within different polyurethanes are less studied, creating a gap in the rational design of new NO releasing devices involving polyurethane materials. Herein, we study the diffusion and partitioning of NO in different biomedical polyurethanes via the time-lag method. The diffusion of NO is positively correlated with the PDMS content within the polyurethanes, which can be rationalized by effective media theory considering various microphase morphologies. Using catheters as a model device, the effect of these transport properties on the NO release profiles and the distribution around an asymmetric dual lumen catheter are simulated using finite element analysis and validated experimentally. This method can be readily applied in studying other NO release medical devices with different configurations.

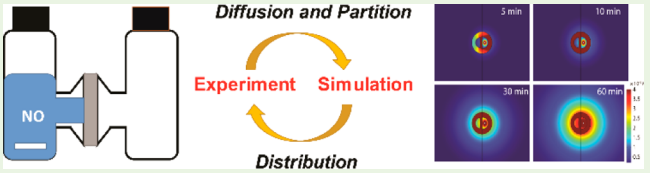

KEYWORDS: *nitric oxide, mass transport, distribution, finite element analysis, medical devices, polyurethanes*

INTRODUCTION

Biocompatibility is central to the design and performance of medical devices. The issues of biocompatibility include clot formation on blood contacting devices,[1] foreign body response on subcutaneous implants,[2] biofilm formation, and microbial infections on all types of invasive devices.[3] One promising means to combat all of these issues with a single agent is to employ nitric oxide (NO), which is endogenously produced in the body. In the bloodstream, NO can prevent thrombosis by inhibiting platelet adhesion and activation, while in soft tissues, NO can promote wound healing.[4−7] It is also a potent antimicrobial/antibiofilm agent. These versatile properties are desirable for medical devices, for example, catheters. However, because NO is a gas molecule and is relatively reactive, the use of NO donors together with proper release methods are necessary to deliver NO locally to be effective clinically.[8] Nitric oxide donors can either be covalently attached to, or noncovalently incorporated within polymers,[9,10] and such polymers are then applied either as coatings for devices, including intravascular sensors, or as the bulk material of the devices (e.g., catheters, intravascular sensors, and stents).[11−13]

Two types of biomedical polymers, silicone rubber[14−17] and polyurethanes,[18−21] are extensively used in creating NO releasing materials because of their innate compatibility with NO release chemistry, appropriate mechanical properties and high stability in vivo.[22] However, the transport properties of such polymers with respect to NO diffusion rates, partition coefficients, etc., have been less studied. Such transport properties not only can significantly impact the NO release profile, including surface flux of NO, the longevity of release, and time required to reach steady-state release, but also can affect the distribution of NO release around the surface of actual devices. On the other hand, such transport properties, once known, can help predict the NO release profile and NO distribution around the devices made of certain polymers, ultimately guiding the optimal design/configuration of devices for biomedical applications.

Mowery et al. examined the transport of NO in polymers and obtained apparent diffusion coefficients for NO in PVC, silicone rubber, and two aliphatic polyether polyurethanes.[23] Although useful in predicting the average flux at steady-state, transient processes, local flux distribution, and transport processes coupled with chemical reactions cannot be accurately described using apparent diffusion coefficient values alone. This is because this apparent diffusion coefficient represents the mixed processes of diffusion and partitioning. Polymers with same apparent diffusion coefficient can display very different NO release profiles and distributions. Moreover, the transport properties of NO in newly developed polyurethanes that have been shown to exhibit improved stability and biocompatibility in vivo have not been reported.[24]

Received: April 22, 2016
Accepted: July 27, 2016
Published: July 27, 2016

DOI: 10.1021/acsbiomaterials.6b00215
ACS Biomater. Sci. Eng. 2016, 2, 1483−1492

To better understand the time-dependent NO transport and release processes in biomedical polyurethanes and to improve the design of NO releasing scaffolds and devices, in this study, the transport properties of NO in different polyurethanes, including classic aliphatic, aromatic polyether polyurethanes, as well as novel silicone and polycarbonate containing polyurethanes, are examined. The true diffusion coefficients of NO in these polymers are separated from the partition process. Finally, the effects of varied diffusion and partitioning on the NO release profile as well as the distribution of NO at the surface of multilumen catheters are simulated using finite element analysis and compared with experimental results.

THEORY

Gas Transport in Polymers: Diffusion and Solution. Transport of gas through polymers can be described by two different processes—diffusion and solution. Here, solution is the process of gas partitioning between the polymer phase and the gas or liquid phase, and therefore the term partition and solution are used interchangeably in this paper. Figure 1 summarizes a general 1D model for NO permeation from one stream (upstream) into another stream (downstream) through a polymer layer, which can describe the diffusion experiments conducted in this study, as well as NO release process from a NO reservoir inside a polymeric membrane, e.g., electrochemical (e-chem) NO release system.[24−26]

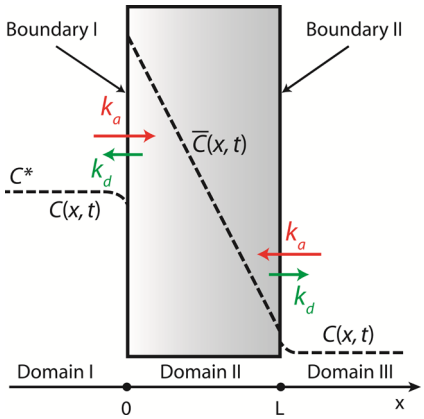

Figure 1. Schematic for NO transport through a polymer film/wall with a thickness of L. Dashed line indicates the concentration profile of NO.

Suppose gas molecules dissolved in a solution (Domain I) with bulk concentration C^* permeate through a polymeric membrane (Domain II) to the downstream solution on the other side of the membrane (Domain III) because of the concentration gradient (see Figure 1). First, the dissolved gas in Domain I is transported to close proximity to the polymer/solution interface (Boundary I) by diffusion (diffusion coefficient D) and convection. Second, the gas molecules close to the interface (Boundary I) partition between the polymer and solution phases. This partitioning process can be viewed as two elementary steps: adsorption (transfer from solution into polymer, with a heterogeneous rate constant k_a), and desorption (transfer from polymer into solution, with a heterogeneous rate constant k_d). The ratio of k_a/k_d determines the partition coefficient K between the two phases. In the third step, the gas molecules that have partitioned into the polymer membrane (Domain II) are transported to the other interface of the membrane (at $x = L$) by diffusion (diffusion coefficient $\bar{D}$; the bar denotes the membrane phase). The fourth step involves again the partition between polymer/solution interface (Boundary II) with the same k_a and k_d as in the second step. Finally, the gas molecules that have entered the receiving solution (Domain III) will be transported away. The driving force for all these processes is the chemical potential gradient, or equivalently, the concentration gradient.

Several assumptions are made to simplify the mathematical model for the diffusion process shown in Figure 1. First, we assume that all the diffusion processes are Fickian (i.e., magnitude of the flux is proportional to the concentration gradient, and diffusion coefficient is concentration independent). This assumption is valid as the gas molecule is small and the concentration of gas in the experiment is low, ensuring no significant change of the polymer, structurally or dynamically, by the presence of the diffusing gas molecules (i.e., no swelling or plasticization). Second, the membrane is isotropic and homogeneous. This should be macroscopically true for the polymers under study. On the basis of these assumptions, diffusion equations in the three domains coupled by partitioning in 1D as well as the corresponding initial values and boundary conditions are shown below

Domain I

$$\frac{\partial C(x, t)}{\partial t} = D\frac{\partial^2 C(x, t)}{\partial^2 x} \quad (1)$$

$$C(-\infty, t) = C(x, 0) = C^* \quad (2)$$

$$J(0, t) = k_d\bar{C}(0, t) - k_a C(0, t)$$

$$= k_d[\bar{C}(0, t) - KC(0, t)] \quad (3)$$

Domain II:

$$\frac{\partial \bar{C}(x, t)}{\partial t} = \bar{D}\frac{\partial^2 \bar{C}(x, t)}{\partial^2 x} \quad (4)$$

$$\bar{J}(0, t) = -J(0, t) = k_d[KC(0, t) - \bar{C}(0, t)] \quad (5)$$

$$\bar{J}(L, t) = [k_a C(L, t) - k_d\bar{C}(L, t)]$$

$$= k_d[KC(L, t) - \bar{C}(L, t)] \quad (6)$$

$$C(x, 0) = 0 \quad (7)$$

Domain III:

$$\frac{\partial C(x, t)}{\partial t} = D\frac{\partial^2 C(x, t)}{\partial^2 x} \quad (8)$$

$$J(L, t) = -\bar{J}(L, t) = k_d[\bar{C}(L, t) - KC(L, t)] \quad (9)$$

$$C(+\infty, t) = C(x, 0) = 0 \quad (10)$$

Equations 1, 4, and 8 are diffusion equations in the different domains, and the other equations are initial values and boundary conditions. Equations 3 and 5, and eqs 6 and 9 couple the diffusions in Domains I, II and Domains II, III, respectively, by enforcing continuous fluxes across the boundaries.

For the diffusion experiment, assuming stirring provides sufficient mixing in Domain I, the concentration of NO in solution can be treated as homogeneous. The large amount of solution volume in Domain I as compared to the membrane volume (Domain II) ensures that bulk concentration of NO in Domain I remains essentially constant during a typical diffusion experiment. The homogeneity and time invariance of NO concentration simplifies eqs 1 and 2 to

DOI: 10.1021/acsbiomaterials.6b00215
ACS Biomater. Sci. Eng. 2016, 2, 1483−1492

$$C(x, t) = C^*, \text{ for } x < 0 \quad (11)$$

Assuming fast equilibrium of partition at the interface, eqs 3 and 5 can be reduced to

$$\bar{C}(0, t) = KC(0, t) = KC^* \quad (12)$$

Similarly, because NO in the downstream (Domain III) is rapidly pumped into the detector for measuring the rate of NO transport, or scavenged very quickly by oxyhemoglobin when practically using NO release devices in contact with blood, the concentration of NO in Domain III is essentially zero at all times. eqs 8 and 10 are therefore reduced to

$$C(x, t) = 0, \text{ for } x > L \quad (13)$$

And by analogy for fast equilibria, eqs 6 and 9 become

$$\bar{C}(L, t) = KC(L, t) = 0 \quad (14)$$

Under these conditions, the complicated coupled diffusion in three domains is now simplified into the diffusion process in Domain II alone, with governing eq eq 4 and boundary conditions provided by eqs 12 and 14 and initial value, eq 7.

Such diffusion equations can be solved exactly, and integrating the flux at $x = L$ over time yields

$$Q(L, t) = \frac{\bar{D}KC^*}{L}\left(t - \frac{L^2}{6\bar{D}} + \frac{2L^2}{\pi^2\bar{D}} \sum_{n=1}^{\infty} \frac{(-1)^{n+1}}{n^2} \exp\left(-\frac{\bar{D}n^2\pi^2 t}{L^2}\right)\right) \quad (15)$$

where $Q(L, t)$ is the accumulated amount of gas that penetrates the membrane per unit area at time t. When $t \to \infty$, the exponential term is dropped

$$Q(L, t) = \frac{\bar{D}KC^*}{L}\left(t - \frac{L^2}{6\bar{D}}\right) \quad (16)$$

Therefore, plot of the amount of permeated gas versus time will approach a linear asymptote as $t \to \infty$, with an intercept at the x-axis

$$\tau = \frac{L^2}{6\bar{D}} \quad (17)$$

τ is defined as the time lag. Once the membrane thickness L and time lag τ are obtained, the diffusion coefficient can be calculated from eq 17.

The first derivative of eq 15 with respect to time gives

$$J(L, t) = \frac{\bar{D}KC^*}{L} + \frac{2\bar{D}KC^*}{L} \sum_{n=1}^{\infty} (-1)^n \exp\left(-\frac{\bar{D}n^2\pi^2 t}{L^2}\right) \quad (18)$$

The first term of eq 18 corresponds to the steady-state portion of the flux, whereas the second term corresponds to the transient portion of the flux. As $t \to \infty$, the flux reaches steady-state:

$$J_{ss}(L) = \frac{\bar{D}KC^*}{L} \quad (19)$$

From the steady-state flux J_{ss}, the product of $\bar{D}K$ can be obtained. Together with the $\bar{D}$ obtained from the transient time lag, the partition coefficient K can be derived. This forms the basis for measurement of both the diffusion coefficients and partition coefficients of NO in this study for a variety of biomedical polymers.

Under other conditions, for example, electrochemical NO generation from catheters,[26,27] the assumption of effective stirring in Domain I is no longer valid and a significant diffusion layer will exist within the inner source solution phase. To solve this more complicated problem, diffusion equations in Domain I and II need to be coupled together. Distribution of NO around an actual catheter surface is also of interest during the application of these type of devices. For this purpose, however, the 1D model is not sufficient to describe the distribution process. This complicated case can be solved in higher dimension numerically using finite element analysis, which is described in the next section.

EXPERIMENTAL SECTION

Materials and Instrument. Sodium nitrite (99.99%), potassium iodide, and sulfuric acid were purchased from Sigma-Aldrich (St. Louis, MO) and used as received. All the solutions were prepared with deionized water from a Milli-Q system (18 MΩ cm^{-1}; Millipore Corp., Billerica, MA).

Carbosil 20 80A and Bionate 80A were from DSM (Heerlen Netherlands), while Elast-Eon 5−325 80A (E5−325) was from AorTech International plc (Weybridge, UK). Tecoflex SG-80A and Pellethane 80AE were gifts from Lubrizol (Cleveland, Ohio). Silicone rubber sealant (RTV-3140) was a product of Dow Corning (Midland, MI).

Membrane Preparation. All the polyurethane films were prepared by casting a 10 wt % solution of the polymer in THF in a 6 cm diameter glass O-ring on a glass slide. The slide was left to dry in a fume hood for 24 h and then placed under vacuum for further drying for another 4 h period. Silicone rubber films were prepared by casting a suspension of RTV sealant in THF within a 6 cm Teflon O-ring on a Teflon slide with 48 h drying under ambient conditions. The chemical composition selective and properties of all the polymers used in this study are listed in Table S1.

NO Transport Measurements. In a homemade diffusion cell, a membrane was clamped in between the two parts of the cell (see Figure S1 for the experimental setup). The temperature of the cell was controlled by a water bath. The NO was generated from one part of the cell reproducibly via quantitative conversion of nitrite to NO in the presence of acid and reducing agent (e.g., $2\,NO_2^- + 2\,I^- + 4\,H^+ \rightarrow 2\,NO + 2\,H_2O + I_2$) as reported previously.[28] Briefly, solutions of 0.1 M H_2SO_4 and 5% KI were prepurged with N_2 for 20 min to remove O_2. A 3.5 mL aliquot of each solution was then added to the left side of the diffusion cell. Each side of the cell was purged thoroughly with N_2 again for another 20 min to eliminate O_2. The solution on the left side was then vigorously stirred throughout the entire time of the experiment. Then, the time was recorded when a 50 μL aliquot of a $NaNO_2$ standard solution (5 mM) was injected into the 7 mL solution on the left side of the cell. The NO flux was measured in real time with chemiluminescence using a nitric oxide analyzer (NOA) (Sievers 280i, GE Analytics, Boulder CO) until the steady-state flux was reached.

Alternatively, 0.1 M H_2SO_4 and 5% freshly made ascorbic acid can also be used to generate NO from nitrite solutions when I_2 adsorption was found to be significant on the polymer surface (for Carbosil 20 80A).

Fabrication of Electrochemical NO Releasing Silicone and Polyurethane Catheters. Standard silicone tubing was purchased from VWR. Polyurethane catheter tubing was prepared by dip coating of a 15 wt % of Tecoflex SG80A in THF on a 2.0 mm diameter straight stainless steel mandrel (McMaster-Carr, IL). The tubing obtained had a wall thickness of ~0.3 mm and were cut off for the fabrication of the electrochemical NO releasing catheters. The procedures for the fabrication of the electrochemical NO releasing catheters were similar as previously reported.[24,27] Briefly, the catheter tubing was filled with an aqueous solution of 0.4 M $NaNO_2$, 1 mM copper(II)- 1,4,7-trimethyl-1,4,7-triazacyclononane, 0.15 M NaCl, and 0.5 M HEPES buffer (pH

DOI: 10.1021/acsbiomaterials.6b00215
ACS Biomater. Sci. Eng. 2016, 2, 1483−1492

7.3) using a microsyringe after one end of the catheter was sealed using polyurethane/THF solution (15 wt %). A Teflon-coated Pt wire and a Teflon-coated Ag/AgCl wires were exposed 3 and 6 cm at the tip, respectively. The Ag/AgCl wire was coiled onto the Teflon coating of the Pt wire, and both wires were inserted into the catheter. The other opening of the catheter was then sealed with the same polyurethane/THF solution (15 wt %).

Measurement of Asymmetric Release of NO by Agar Immobilization. An electrochemical NO releasing catheter was mounted on a glass slide with tape. A heat melted 1% agar solution was poured onto a glass slide with four additional glass coverslips forming a container, and the agar incorporated the catheter when cold. The agar was further cut so that the cross-section geometry was rectangular (6 cm × 1 cm, W × H) with the catheter in the center. The NO release was then turned on, and the cumulative amount of NO at each side of the catheter was quantified by measuring the nitrite content using chemiluminescence. Briefly, a piece of the agar sample (6 cm × 1 cm × 2 cm, W × H × L) was dissolved in DI water, and aliquots of the solution were injected into a cell containing degassed 5% KI and 0.1 M H_2SO_4 solution to convert nitrite to NO. The cell was connected to a nitric oxide analyzer for NO measurement via chemiluminescence. The data at each time point are triplicate.

Simulation Methods. Finite element analysis via Comsol Multiphysics (5.0b) was used to simulate the effect of partition coefficient and diffusion coefficient on the NO release profiles when using single lumen catheters and the NO distribution when employing multilumen catheters.

For response time estimation, a 2-D model of the cross-section of a single lumen catheter was implemented. Similar 2-D equations for diffusion coupled by partition as described in eqs 1 (4) (8) and (3) (5) (6) (9) are the governing equations for this transport study, except the Neumann boundary condition of constant flux at the electrode surface was used instead of constant concentration. In Domain III, an NO sink at 0.2 mm away from the catheter surface was purposely set to mimic the fact that NO is removed from the surface of the catheter very fast, either into the NOA by purging, or reacting with oxyhemoglobin when placed within the bloodstream in vivo. For simulation of the distribution of NO around the outer surface of multilumen catheters, a similar model was used except that the cross-section geometry was different. The cross-section geometries of the different catheter models used are shown in Figure 2, and the related parameters are reported in Table S2.

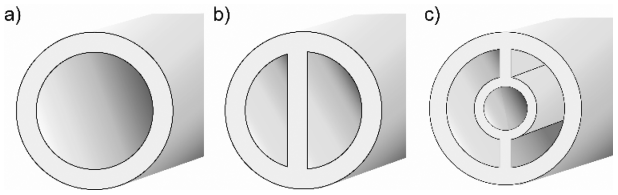

Figure 2. Cross-section geometries for (A) single lumen, (B) commercial dual lumen, and (C) proposed triple lumen catheter studied by finite element analysis.

RESULTS AND DISCUSSION

Diffusion Studies of NO Through Polyurethanes. A typical plot of NO flux (J_{NO}) and the accumulative amount of permeated NO (Q_{NO}) vs time for NO diffusion through an E5−325 polyurethane membrane is shown in Figure 3. From the steady-state flux, together with membrane thickness, $\bar{D}K$ can be obtained according to eq 19. The accumulated amount of the permeated NO (Q_{NO}) vs time can be used to estimate time lag (τ) and calculate the diffusion coefficient. Similar experiments were performed for the other polyurethanes and silicone rubber films (structure description and selected physical properties of all the polymers under investigation are listed in Table S1) at both

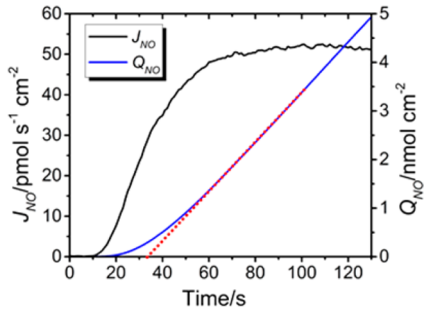

Figure 3. Typical NO flux profile (J_{NO}, black) and amount of permeated NO (Q_{NO}, blue) vs time for a 368 μm E5−325 polyurethane film at 25 °C in a diffusion experiment. Red dotted line denotes the asymptote used for deriving the time lag (τ).

25 and 37 °C. The measured diffusion coefficient and partition coefficients of NO in these polymers are summarized in Table 1.

The diffusion coefficient of NO ($\bar{D}$) determined in the different polymers is negatively correlated to the density (ρ) of the polymer (see Table S1). This can be understood by the free volume theory,[30] in which the polymer is considered to be a combination of hard and soft segments. The transport through the soft segment is a dominant pathway for the gas to diffuse through the polymer. Some authors have referred to the regions of soft segment within the hard segment structures as holes, and describe diffusion in a polymer as "hopping" between the "holes" of free volume,[31] with the relationship

$$\log \bar{D} = A - \frac{B}{f_v} \tag{20}$$

where A and B are constants related to the size of the penetrants and the hole size of the polymer matrix, respectively, and f_v is the fraction of the free volume. Assuming similar densities of different polymer chains (occupied volumes) in this study, the specific density of a polymer is negatively proportional to f_v (Figure S2). In fact, a direct relationship between f_v and $\bar{D}$ has been established experimentally by diffusion and positron annihilation lifetime experiments.[31]

From the diffusion study, silicone rubber has the highest $\bar{D}$ for NO, and all the polyurethanes containing PDMS segments examined in this study exhibit significantly higher diffusion coefficients for NO than similar polyurethanes without the PDMS segments (e.g., E5−325 vs Pellethane, Carbosil vs Bionate, see the detailed structure information in Table S1). This is because that the PDMS chain is flexible with a low rotation barrier, which allows for a large free volume and therefore fast diffusion for penetrants like NO. The large free volume of PDMS chain is also indicated by the low glass transition temperature (T_g) of neat PDMS (−112 °C).[32]

The relatively slow diffusion of NO in Bionate and Carbosil can be attributed to the interaction between the polycarbonate chain and the urethane moiety. Although the polycarbonate chains, (poly(1,6-hexyl 1,2-ethyl carbonate) (PHEC), exhibit a relatively low T_g of −70 °C in the neat form, they can form strong hydrogen bonds with the urethane moieties in polyurethanes.[32] Such hydrogen bonding significantly decreases the free volume by a closer packing of the polymer chains and a reduction in chain mobility, which is also indicated by the much higher T_g (−7 °C) of the PHEC segments in polycarbonate copolymers of polyurethanes.[32] This reduced free volume of PHEC chains in polyurethanes and decrease the diffusion of NO in these polymers.

DOI: 10.1021/acsbiomaterials.6b00215
ACS Biomater. Sci. Eng. 2016, 2, 1483−1492

Table 1. Summary of Diffusion Coefficients ($\bar{D}$) and Partition Coefficients (K) of NO in Various Polymers at 25 and 37 °C Obtained in This Study[a]

polymer	description	thickness (μm)	$\bar{D}_{25\ °C}$ ($\times 10^{-6}$ cm^2 s^{-1})	$\bar{D}_{25\ °C}$ ($\times 10^{-6}$ cm^2 s^{-1})	$K_{25\ °C}$	$K_{37\ °C}$
Silicone	silicone rubber	1107 ± 16	16 ± 2	20 ± 4	5 ± 1	4 ± 1
Elast-Eon 5−325	silicone polyurethane	621 ± 10	6 ± 1	8.5 ± 0.8	3.8 ± 0.5	3.3 ± 0.3
Tecoflex SG80A	polyether polyurethane	437 ± 10	1.2 ± 0.5	1.9 ± 0.5	2.5 ± 0.8	2.2 ± 0.3
Carbosil 20 80A	silicone polycarbonate polyurethane	442 ± 8	0.7 ± 0.1	1.4 ± 0.5	1.2 ± 0.4	0.3 ± 0.1
Pellethane 80A	polyether polyurethane	128 ± 4	0.5 ± 0.1	0.8 ± 0.3	1.5 ± 0.4	1.1 ± 0.2
Bionate 80A	polycarbonate polyurethane	174 ± 4	0.3 ± 0.1	0.7 ± 0.1	0.7 ± 0.2	0.6 ± 0.1

[a] n = 3 replicates. Results are reported as mean ± standard deviations.

Tecoflex SG80A and Pellethane 80A are both polyurethanes with polyether chains as soft segments but exhibit quite different diffusion properties for NO (see Table 1). Tecoflex SG80A contains urethane segments from 4,4′-methylene-bis(cyclohexyl isocyanate) (HMDI) and 1,4-butanediol (BDO), whereas Pellethane 80A contains urethane segments from 4,4′-methylene-bis(phenyl isocyanate) (MDI) and BDO.[33−35] As the aromatic MDI is more rigid than the aliphatic HMDI, polyurethanes derived from MDI segments have a higher barrier for chain rotation and therefore lower free volume. Therefore, Tecoflex SG80A exhibits a higher diffusion coefficient for NO than Pellethane.

In addition to the chain flexibility and free volume, polymer morphology in block copolymers also significantly affects the diffusion of gas molecules.[36] This is especially true for polyurethanes as they tend to microphase separate into different morphologies, including a continuous phase with spheres, cylinders, and lamellae.[37] The exact morphology depends on the miscibility of the blocks of the copolymer, stoichiometry of the blocks, and the preparation conditions (including thermal history).[38] In polyurethanes with PDMS chain, such as E5−325 and Carbosil, the PDMS segments can undergo phase separation of nearly 100%,[32,39] which allows the fraction of the PDMS phase to be simply represented by the stoichiometry. Effective media theory has been proposed to model diffusion within polymer blends with different morphology, including spheres, cylinders, and lamellae.[40] Such methods were first developed for solving conductivity of composite materials, and the derived equations can be directly applied for diffusion by changing the conductivity into permeability (see the derived equations in the Supporting Information). The diffusion of gas in polyurethanes can be modeled by considering the compositions of cells with morphologies as shown in Figure 4A in random orientations.

E5−325 possesses segments of PDMS and MDI:BDO with the PDMS content as high as 66%. This micromorphology can be described as two phases comprising a continuous PDMS phase (66%) and discontinuous hard segment phase. From Figure 4B, the point for E5−325 lies close to the predicted line for a cylinder of a hard phase in PDMS. However, a volume fraction of 66% is likely to be near the percolation threshold.[41] Predictions near the percolation threshold using this method often involves large error, because of uncertainty whether a percolating network spans the entire material.[42] In the finite element model, the availability of percolating network through the wall of the catheter depnds on morphologies of the mode (Figure 4A), which are idealized. The idealized morphology could lead to erroneous model predictions near the percolation threshold, but it is accurate for other volume fractions because the morphology does not affect the availability of a percolation network.

For Carbosil-20, the PDMS chains phase separate completely because of low compatibility with other chains. From percolation theory, PDMS, with a volume fraction of 20%, is less likely to form a continuous phase. Significant mixing of PHEC and the hard segment occurs, and only 10−15% of hard segment phase is separated (~4% of total volume).[32] The small amount of separated hard segment phase can be neglected to simplify the description as a two-phase model. The morphology is, therefore, described as a continuous PHEC/hard segment mixed phase with islands of PDMS. From Figure 4C, Carbosil-20 is likely to contain a lamellae structure of the PDMS phase and the PHEC/hard segment mixed phase.

In this study, diffusion coefficients and partition coefficients of NO were obtained only at 25 and 37 °C as these temperatures are

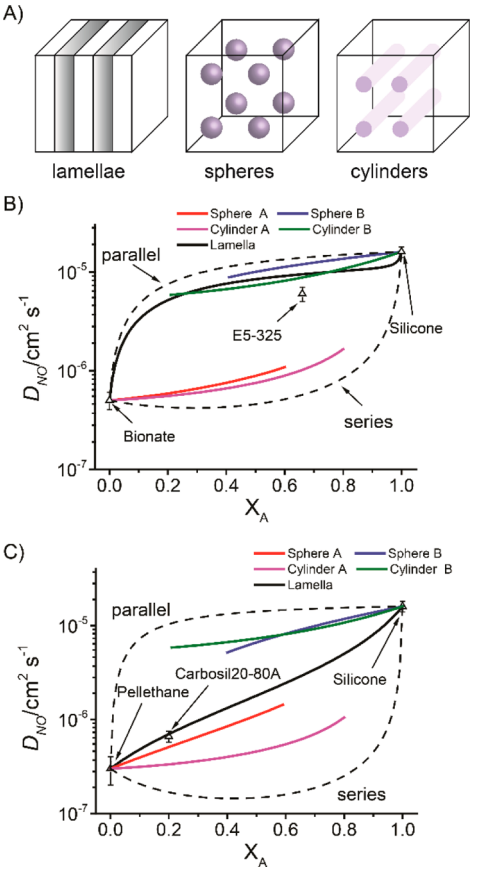

Figure 4. Effect of volume fraction of PDMS in polyurethanes on the diffusion coefficient of NO from experiment and modeling. A) Cells of typical morphology (lamellae, spheres, and cylinders) for block copolymers with phase separation used for modeling; Predicted (lines) and experimentally obtained (triangles, error bars denote standard deviations from n = 3) diffusion coefficient of NO (D_{NO}) vs volume fraction of PDMS (X_A) based on different morphologies for B) silicone polyurethanes and (C) silicone polycarbonate polyurethanes.

DOI: 10.1021/acsbiomaterials.6b00215
ACS Biomater. Sci. Eng. 2016, 2, 1483−1492

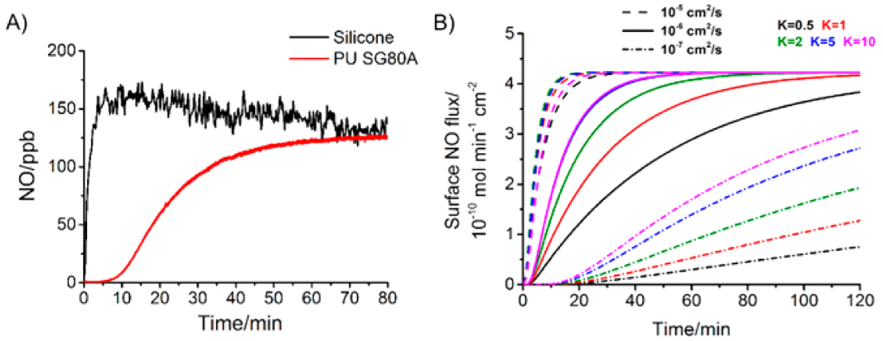

Figure 5. NO release profile for electrochemical NO releasing catheters (0.3 mm wall thickness, 2.6 mm o.d.). A voltage of −0.3 V was applied at time 0 to generate a steady flux of NO from the electrode surface. A) Experimental data from single-lumen catheters made from silicone (black) and Tecoflex SG80A (red); B) Simulation of the effect of diffusion and partition on NO release profile from electrochemical NO releasing catheters.

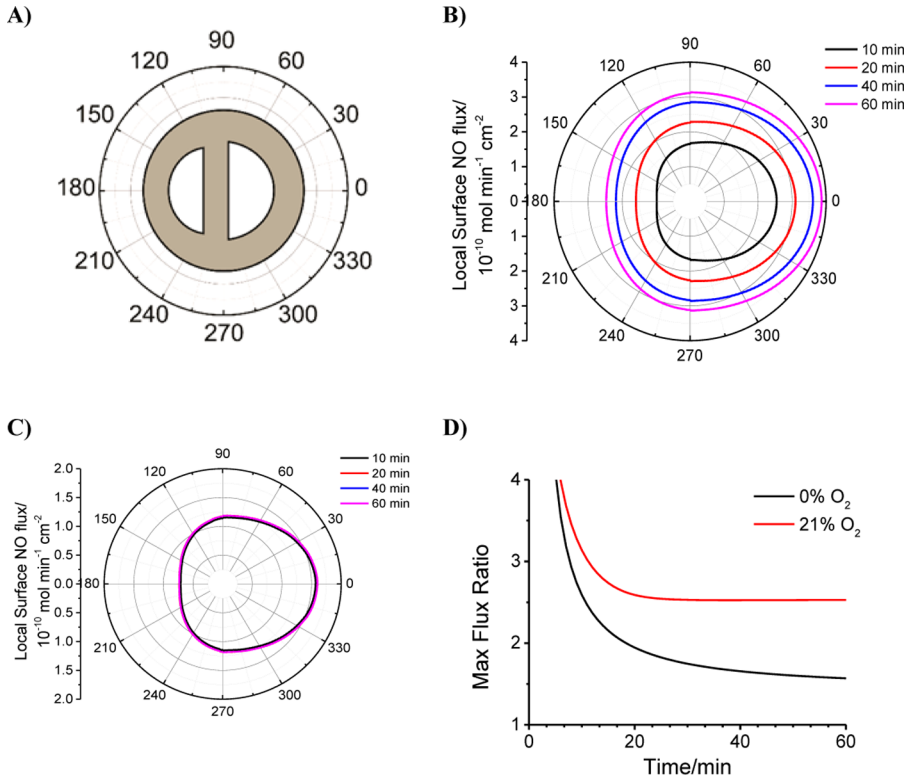

Figure 6. Local flux of NO on surface of a 7-Fr Cook dual lumen silicone catheter at room temperature in N_2 and in air. A) illustration of the polar angle for the dual lumen catheter; B) polar graph showing the local surface flux vs time with 0% and C) 21% O_2; D) Maximum surface flux ratio vs time under 0 and 21% O_2.

most relevant for biomedical applications. As expected, the diffusion coefficients of NO increase for all the polymers tested when the temperature increases (see Table 1). However, we did not attempt to derive an apparent Arrhenius activation energy from the two temperature data points. Such an activation energy would contain contributions from both the diffusant (NO) and the polymer and is less useful considering the complex compositions and phase transitions of the different polymers at different temperatures.

Errors in the diffusion experiments stem from many factors with major ones being the measurement of the thickness of the membranes, the uncertainty from the response time of the NO measurement (~2 s), and the effectiveness of convection by stirring the NO generating solution. During the diffusion experiment, asymmetry exists as one side of the membrane is contacting an aqueous phase (Domain I in Figure 1), whereas the other side is contacting a gas phase (Domain III in Figure 1). Such asymmetry could potentially affect the adsorption and desorption processes (by changing the local structure near the interfaces). In this experiment, the adsorption and desorption processes have been assumed to occur very fast for both the water/polymer interface and the gas/polymer interface and, therefore, can be negligible. Indeed, diffusion experiments with different thickness of membranes yield very similar diffusion coefficients, suggesting that the surface process is not rate limiting. The purpose of having a gas phase instead of a solution on the other side is to minimize the response time for the NO detection and to ensure an effective zero concentration of NO in the by quickly forcing the arriving NO into the detector.

Effect of Diffusion and Partition on Response Time of NO Release. Partition and diffusion describe NO transport in polymers and therefore affect the NO release profile of some NO

DOI: 10.1021/acsbiomaterials.6b00215
ACS Biomater. Sci. Eng. 2016, 2, 1483−1492

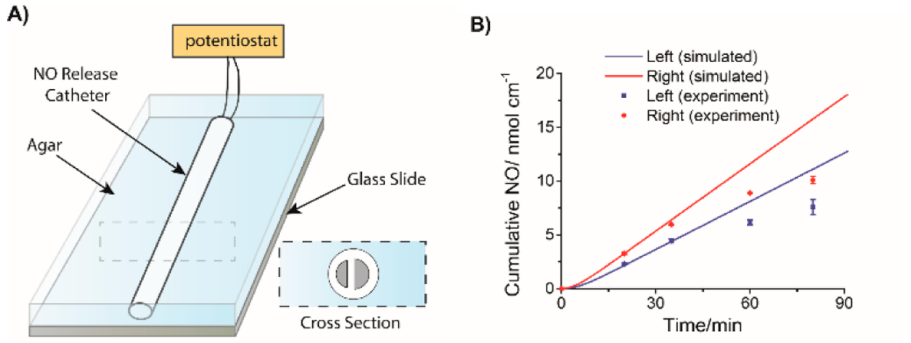

Figure 7. Experiment probing the distribution of NO by around a dual lumen catheter. A) Experimental setup of catheter immobilization using agar; B) cumulative NO in the left and right domain of the catheter as measured by the agar immobilization experiment (dot) and simulation (line). The error bars indicate standard deviations from $n = 3$ samples. Pearson's R^2 is 0.960 for red curve and 0.957 for blue curve.

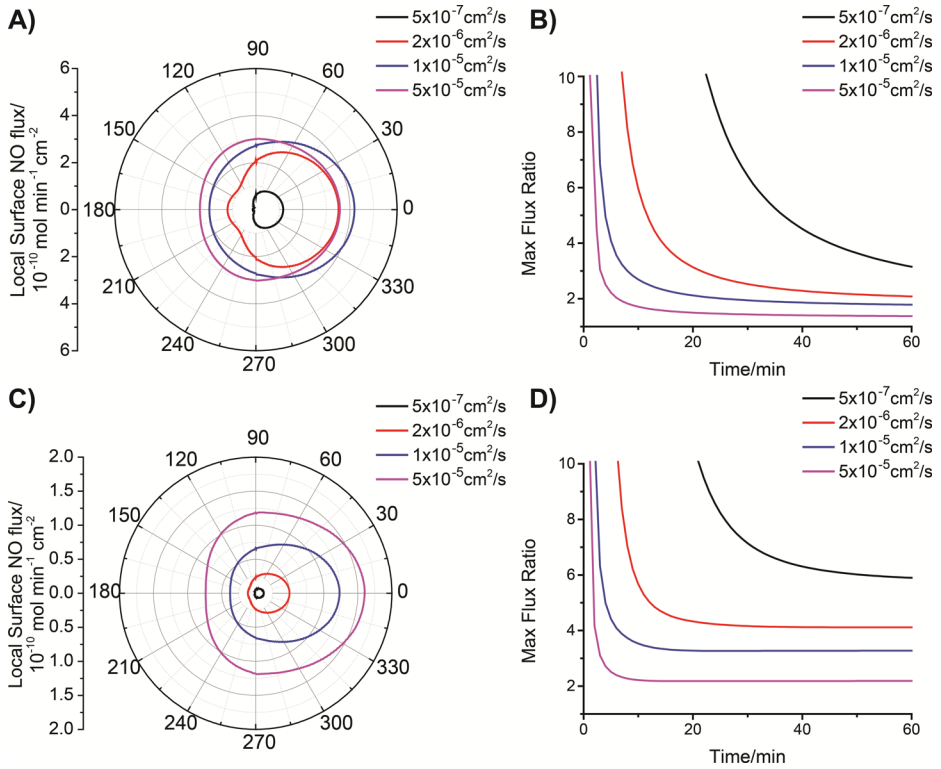

Figure 8. Effect of different diffusion coefficients ($\bar{D}$) on the distribution/asymmetry of NO on a dual lumen catheter (same configuration and polar angle as shown in Figure 6A) over time with $K = 2.5$. A) Polar graph showing the distribution of local NO flux at the catheter surface at 0% O_2; B) maximum flux ratio vs time with 0% O_2; C) Polar graph showing the distribution of local NO flux at the catheter surface with 21% O_2; D) maximum flux ratio vs time with 21% O_2.

release materials/systems. For example, the duration for the NO release to reach steady-state release, defined as response time, is of importance as it can affect the performance and the use of NO releasing devices. Catheters made from silicone and Tecoflex SG 80A with electrochemical NO release system are used in this work to demonstrate such an effect. The electrochemical NO generation system can produce a steady flux of NO from the electrode surface with constant voltages, which can release from the catheter surface via diffusion through the inner filling solution and the wall of the catheter. Such NO releasing catheters made from different materials with the same geometry show very different release profiles. As seen in Figure 5A, for a silicone catheter, the surface flux of NO reaches a steady state within 5 min after the NO release is turned on, whereas for a catheter made from Tecoflex SG80A, it takes more than 60 min to reach the steady-state release. This is explained by the fact that the diffusion coefficient of NO in silicone is 13 times greater than that in Tecoflex SG80A (see Table 1).

To obtain the more general effects of diffusion and partition on NO release from single lumen catheters, we applied finite element analysis (using Comsol Multiphysics) to simulate the surface NO flux after NO is turned "on" for the electrochemical NO releasing catheters. From the simulation, the response time of NO release becomes smaller as $\bar{D}$ and K increase (see Figure 5B). This simulation result together with $\bar{D}$ and K obtained in the diffusion study (Table 1) immediately suggests that silicone and E5−325 is the preferred material for electrochemical NO releasing catheters in terms of response time. For a typical single lumen catheter with 0.3 mm wall thickness, the response time for silicone and E5−325 will be ≲20 min.

DOI: 10.1021/acsbiomaterials.6b00215
ACS Biomater. Sci. Eng. 2016, 2, 1483−1492

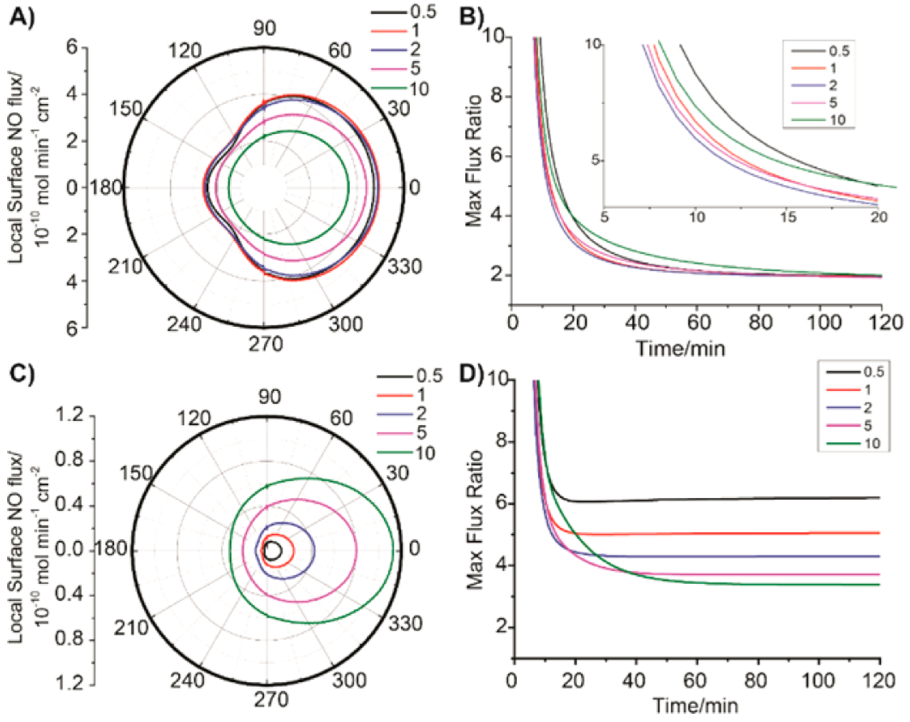

Figure 9. Effect of partition coefficient (K) on the distribution of NO for a 7-Fr Cook dual lumen catheter at 20 min in 0% O_2 and 21% O_2. Diffusion coefficient $\bar{D} = 2 \times 10^{-6}$ cm^2 s^{-1}. A) Polar graph showing the distribution of NO flux at catheter surface without O_2; B) maximum flux ratio vs time without O_2; C) Polar graph of showing the distribution of NO flux at catheter surface with 21%; D) maximum flux ratio vs time with 21% O_2.

The other polyurethanes with low $\bar{D}$ and K values, although not ideal for direct application in electrochemical NO release catheter, could be potentially used as release barriers to slow down the NO release and mitigate burst release in many NO release materials, and to prolong the lifetime NO release. Indeed, drug delivery using nanoparticles, where prolonged release is often hard to achieve, calls for materials with low permeability as the outer barrier.[43]

Effect of Diffusion and Partition on Distribution of NO for Multi-Lumen Catheters. Another aspect of NO release is the distribution of NO release on the surface of the devices. For example, in clinical practice, the application of electrochemical NO release in catheters requires the use of multilumen catheters because one of the lumens needs to be dedicated for the electrochemical NO generation system. However, as most commercial multilumen catheters are not centrosymmetric, NO distribution around the outer surfaces of such catheters can be asymmetric. Depending on the severity, such asymmetry can potentially create problems (e.g., one side of the device being less biocompatible than the other). On the other hand, polymers with a high partition coefficient could serve as a reservoir for NO release and could promote a more symmetrical distribution of NO when coupled with a high diffusion coefficient. Both $\bar{D}$ and K, besides the geometry of the inherently asymmetric device, could impact the distribution of NO.

To study such asymmetry effect, as a first step, a commercial dual lumen silicone catheter was simulated using $\bar{D}$ and K values obtained in this study with NO release electrode in the right lumen (cross-section geometry of this catheter is shown in Figure 6A). Such a catheter has already been used in antithrombotic, antimicrobial studies as well as in preparing the new NO release PO_2 sensing catheters.[26,27,29] The local surface flux distribution on the catheter surface over time with 0% O_2 (no sink for NO) is plotted in Figure 6B. It can be seen that a significant asymmetry exists initially (e.g., at 10 min), which can be also observed in the concentration color map in Figure S3. To quantify the worst-case scenario of the asymmetry, we used the ratio of the highest to the lowest local fluxes on the surface and termed it as the maximum flux ratio thereafter. For this dual lumen silicone catheter, the maximum surface flux ratio decreases to <2 after 20 min in the absence of O_2 (Figure 6D). With ambient O_2 reacting with NO (as a sink for NO), the surface flux reaches a steady-state after 30 min (Figure 6C), and the maximum ratio of surface flux reaches 2.5 (Figure 6D). Such asymmetry was also probed experimentally by measuring the cumulative nitrite content at different sides of the catheter in an agar gel (released NO reacts with O_2 to form nitrite that stays in the agar) into which electrochemical NO releasing catheter was placed. A schematic for the experimental measurement of the asymmetry is shown in Figure 7A. As shown in Figure 7B, the cumulative NO from the nitrite measurement agrees well with that from simulation with a correlation coefficient (Pearson's R^2) of 0.960.

To continue using this commercial dual-lumen catheter as an example, the more general effect of diffusion and partition (in the relevant range) on the asymmetry of NO distribution was further studied by simulation. The lowest diffusion coefficient in the simulation ($\bar{D} = 5 \times 10^{-7}$ cm^2 s^{-1}) shows the most asymmetric distribution of surface NO flux, with a maximum surface flux ratio of >10 (see Figure 8A). Such a large asymmetry is partially a transient effect as the low diffusion coefficient cause the NO to permeate one side of the catheter (the right side of the catheter in Figure 6A) before a significant amount appears on the other side. The symmetry is enhanced over time, but the enhancement is much faster for larger diffusion coefficients (see Figure 8B). Overall, the symmetry is always significantly better when diffusion coefficients are larger. The same trends are also true when the reaction of NO with O_2 is also considered, although the

DOI: 10.1021/acsbiomaterials.6b00215
ACS Biomater. Sci. Eng. 2016, 2, 1483−1492

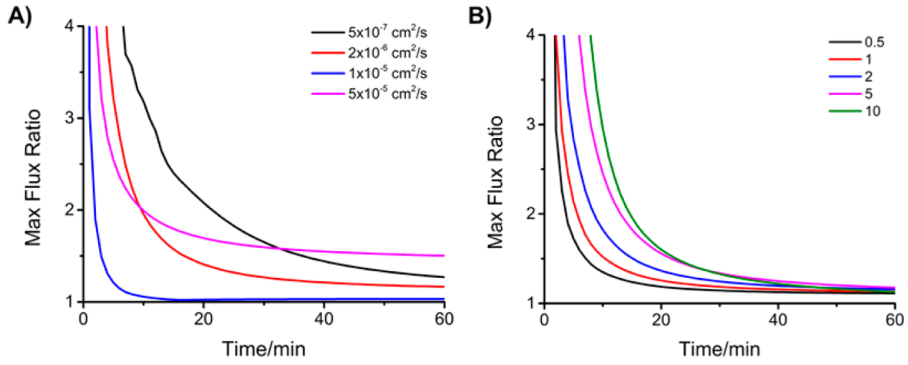

Figure 10. Effect of diffusion coefficient ($\bar{D}$) and partition coefficient (K) of NO in the polymer on the maximum flux ratio of an electrochemical NO releasing catheters with a more symmetric design as shown in Figure 2C (NO releasing electrode in the middle lumen). (A) Maximum flux ratio with various $\bar{D}$ at K = 2; (B) Maximum flux ratio with various K at $\bar{D} = 2 \times 10^{-6}$ cm^2 s^{-1}.

exact symmetry is worse compared to that without the reaction (see Figure 8C, D).

The effect of partition coefficient on the distribution is more complex and is time-dependent. Without O_2, the largest partition coefficient (K = 10; NO partitions favorably in the polymer) yields the lowest average flux of NO and worst distribution at the 20 min (see Figure 9A, B). This is likely because that, with a high partition coefficient, more NO needs to be dissolved in the polymer phase before being released. A partition coefficient of 2 shows the best distribution at all time. With 21% O_2 present, the average surface flux increases as K increases, but the trend for asymmetry vs K changes with time (Figure 9C, D). Within the first 18 min K = 2 offers the best distribution, whereas K = 5 shows the best distribution between 18 and 36 min. After 36 min, a K = 10 exhibits the best distribution. The symmetry stops to change after 70 min for all K, with K = 10 giving the best maximum flux ratio of 3.6 (Figure 9D).

For even better distribution of NO release, a more symmetric design for multilumen catheters is also proposed and investigated by simulation (cross-section geometry is shown in Figure 2C). The distribution of NO around the outer surface is indeed more equal for this more symmetric design; the maximum flux ratio falls below 2 after 20 min for all $\bar{D}$ from 5.0×10^{-7} cm^2 s^{-1} to 5.0×10^{-5} cm^2 s^{-1} at a constant partition coefficient (see Figure 10A). Similarly, the maximum ratio of local surface flux also falls below 2 after 20 min for K ranging from 0.5 to 10 at a constant diffusion coefficient (see Figure 10B).

CONCLUSIONS

Diffusion and partition coefficients for NO in silicone and different biomedical polyurethanes have measured using the time-lag method. The diffusion coefficients for block bi- and tripolymer polyurethanes containing PDMS segments are explained by effective medium theory with different microphase morphologies. The effect of $\bar{D}$ and K on NO release response time as well as asymmetric NO distribution at the outermost surfaces of single and dual-lumen catheters have been examined both experimentally and by simulation. Polymers with large $\bar{D}$ and K for NO exhibit faster response times and catheters made from polymers with large $\bar{D}$ yield enhanced symmetry of NO distribution on the outer surface of the catheter. A more symmetric design for a multilumen catheter is proposed, and the NO distribution is indeed more symmetric for all the partition coefficients and diffusion coefficients being modeled. It should be noted that the transport properties of NO in these biomedical polymers (diffusion and partition) obtained here along with the simulation method demonstrated can be readily applied for the simulation of the more general NO release materials/devices not limited to catheters, by simply inputting the geometry of the devices and the mass transport properties of the materials. Overall, this combination provides a powerful means to design, study, and understand novel NO releasing devices, including the new type of electrochemically generated NO release catheters recently reported by our group.[28,43]

ASSOCIATED CONTENT

Supporting Information

Schematic of the diffusion cell, the relation between density and diffusion coefficient, concentration color map from simulation, chemical properties of the polymers under study, parameters for simulation studies and a brief description of the effective medium theory. The Supporting Information is available free of charge on the ACS Publications website at DOI: 10.1021/acsbiomaterials.6b00215.

(PDF)

AUTHOR INFORMATION

Corresponding Author

*E-mail: mmeyerho@umich.edu.

Notes

The authors declare no competing financial interest.

ACKNOWLEDGMENTS

This work was supported by the National Institutes of Health under NIH-EB-000783 and NIH-R56-HL-119403-01.

REFERENCES

(1) Park, K.; Mosher, D. F.; Cooper, S. L. Acute surface-induced thrombosis in the canine ex vivo model: Importance of protein composition of the initial monolayer and platelet activation. *J. Biomed. Mater. Res.* **1986**, *20* (5), 589−612.

(2) Anderson, J. M.; Rodriguez, A.; Chang, D. T. Foreign body reaction to biomaterials. *Semin. Immunol.* **2008**, *20* (2), 86−100.

(3) Stewart, P. S.; Costerton, J. W. Antibiotic resistance of bacteria in biofilms. *Lancet* **2001**, *358* (9276), 135−8.

(4) Saavedra, J. E.; Southan, G. J.; Davies, K. M.; Lundell, A.; Markou, C.; Hanson, S. R.; Adrie, C.; Hurford, W. E.; Zapol, W. M.; Keefer, L. K. Localizing antithrombotic and vasodilatory activity with a novel, ultrafast nitric oxide donor. *J. Med. Chem.* **1996**, *39* (22), 4361−5.

(5) Fang, F. C. Antimicrobial actions of nitric oxide. *Nitric Oxide* **2012**, *27*, S10.

DOI: 10.1021/acsbiomaterials.6b00215
ACS Biomater. Sci. Eng. 2016, 2, 1483−1492

(6) Bogdan, C. Nitric oxide and the immune response. *Nat. Immunol.* **2001**, *2* (10), 907−916.
(7) Carpenter, A. W.; Schoenfisch, M. H., Nitric oxide release: Part II. Therapeutic applications. *Chem. Soc. Rev.* **2012**, *41* (10). DOI: 374210.1039/c2cs15273h.
(8) Wallis, J. P. Nitric oxide and blood: a review. *Transfus. Med.* **2005**, *15* (1), 1−11.
(9) Frost, M. C.; Reynolds, M. M.; Meyerhoff, M. E. Polymers incorporating nitric oxide releasing/generating substances for improved biocompatibility of blood-contacting medical devices. *Biomaterials* **2005**, *26* (14), 1685−93.
(10) Riccio, D. A.; Schoenfisch, M. H., Nitric oxide release: Part I. Macromolecular scaffolds. *Chem. Soc. Rev.* **2012**, *41* (10). DOI: 373110.1039/c2cs15272j.
(11) Amoako, K. A.; Archangeli, C.; Handa, H.; Major, T.; Meyerhoff, M. E.; Annich, G. M.; Bartlett, R. H. Thromboresistance Characterization of Extruded Nitric Oxide-Releasing Silicone Catheters. *ASAIO J.* **2012**, *58* (3), 238−246.
(12) Schoenfisch, M. H.; Mowery, K. A.; Rader, M. V.; Baliga, N.; Wahr, J. A.; Meyerhoff, M. E. Improving the thromboresistivity of chemical sensors via nitric oxide release: Fabrication and in vivo evaluation of NO-releasing oxygen-sensing catheters. *Anal. Chem.* **2000**, *72* (6), 1119−1126.
(13) Buergler, J. M.; Tio, F. O.; Schulz, D. G.; Khan, M. M.; Mazur, W.; French, B. A.; Raizner, A. E.; Ali, N. M. Use of nitric-oxide-eluting polymer-coated coronary stents for prevention of restenosis in pigs. *Coron. Artery Dis* **2000**, *11* (4), 351−357.
(14) Zhang, H. P.; Schoenfisch, M. H.; Meyerhoff, M. E. Synthesis of nitric oxide releasing silicone rubbers for biomedical applications. *Abstr. Pap. Am. Chem. Soc.* **1999**, *218*, U452−U452.
(15) Frost, M. C.; Rudich, S. M.; Zhang, H.; Maraschio, M. A.; Meyerhoff, M. E. In vivo biocompatibility and analytical performance of intravascular amperometric oxygen sensors prepared with improved nitric oxide-releasing silicone rubber coating. *Anal. Chem.* **2002**, *74* (23), 5942−7.
(16) Zhang, H.; Annich, G. M.; Miskulin, J.; Osterholzer, K.; Merz, S. I.; Bartlett, R. H.; Meyerhoff, M. E. Nitric oxide releasing silicone rubbers with improved blood compatibility: preparation, characterization, and in vivo evaluation. *Biomaterials* **2002**, *23* (6), 1485−94.
(17) Colletta, A.; Wu, J.; Wo, Y.; Kappler, M.; Chen, H.; Xi, C.; Meyerhoff, M. E. S-nitroso-N-acetylpenicillamine (SNAP) impregnated silicone Foley catheters: a potential biomaterial/device to prevent catheter-associated urinary tract infections. *ACS Biomater. Sci. Eng.* **2015**, *1* (6), 416−424.
(18) Reynolds, M. M.; Hrabie, J. A.; Oh, B. K.; Politis, J. K.; Citro, M. L.; Keefer, L. K.; Meyerhoff, M. E. Nitric oxide releasing polyurethanes with covalently linked diazeniumdiolated secondary amines. *Biomacromolecules* **2006**, *7* (3), 987−994.
(19) Coneski, P. N.; Schoenfisch, M. H. Synthesis of nitric oxide-releasing polyurethanes with S-nitrosothiol-containing hard and soft segments. *Polym. Chem.* **2011**, *2* (4), 906−913.
(20) Reynolds, M. M.; Saavedra, J. E.; Showalter, B. M.; Valdez, C. A.; Shanklin, A. P.; Oh, B. K.; Keefer, L. K.; Meyerhoff, M. E. Tailored Synthesis of Nitric Oxide-Releasing Polyurethanes Using O-Protected Diazeniumdiolated Chain Extenders. *J. Mater. Chem.* **2010**, *20* (15), 3107−2114.
(21) Nguyen, E. B.; Zilla, P.; Bezuidenhout, D. *J. Appl. Biomater. Funct. Mater.* **2014**, *12* (3), 172−182.
(22) Lamba, N. M.; Woodhouse, K. A.; Cooper, S. L. *Polyurethanes in biomedical applications*. CRC press: 1997; pp147−180.
(23) Mowery, K. A.; Meyerhoff, M. E. The transport of nitric oxide through various polymeric matrices. *Polymer* **1999**, *40* (22), 6203−6207.
(24) Tanzi, M. C.; Mantovani, D.; Petrini, P.; Guidoin, R.; Laroche, G. Chemical stability of polyether urethanes versus polycarbonate urethanes. *J. Biomed. Mater. Res.* **1997**, *36* (4), 550−9.
(25) Hofler, L.; Koley, D.; Wu, J.; Xi, C.; Meyerhoff, M. E. Electromodulated release of nitric oxide through polymer material from reservoir of inorganic nitrite salt. *RSC Adv.* **2012**, *2* (17), 6765−6767.
(26) Ren, H.; Wu, J.; Xi, C.; Lehnert, N.; Major, T.; Bartlett, R. H.; Meyerhoff, M. E. Electrochemically modulated nitric oxide (NO) releasing biomedical devices via Copper(II)-tri(2-pyridylmethyl)amine mediated reduction of nitrite. *ACS Appl. Mater. Interfaces* **2014**, *6* (6), 3779−3783.
(27) Ren, H.; Colletta, A.; Koley, D.; Wu, J.; Xi, C.; Major, T. C.; Bartlett, R. H.; Meyerhoff, M. E. Thromboresistant/anti-biofilm catheters via electrochemically modulated nitric oxide release. *Bioelectrochemistry* **2015**, *104* (0), 10−16.
(28) Zheng, Z.; Ren, H.; VonWald, I.; Meyerhoff, M. E. Highly sensitive amperometric Pt-Nafion gas phase nitric oxide sensor: Performance and application in characterizing nitric oxide-releasing biomaterials. *Anal. Chim. Acta* **2015**, *887*, 186−91.
(29) Ren, H.; Coughlin, M. A.; Major, T. C.; Aiello, S.; Rojas Pena, A.; Bartlett, R. H.; Meyerhoff, M. E. Improved in vivo performance of amperometric oxygen (PO2) sensing catheters via electrochemical nitric oxide generation/release. *Anal. Chem.* **2015**, *87* (16), 8067−8072.
(30) Fujita, H. Notes on Free Volume Theories. *Polym. J.* **1991**, *23* (12), 1499−1506.
(31) Wang, Z. F.; Wang, B.; Yang, Y. R.; Hu, C. P. Correlations between gas permeation and free-volume hole properties of polyurethane membranes. *Eur. Polym. J.* **2003**, *39* (12), 2345−2349.
(32) Hernandez, R.; Weksler, J.; Padsalgikar, A.; Choi, T.; Angelo, E.; Lin, J. S.; Xu, L.-C.; Siedlecki, C. A.; Runt, J. A Comparison of Phase Organization of Model Segmented Polyurethanes with Different Intersegment Compatibilities. *Macromolecules* **2008**, *41* (24), 9767−9776.
(33) Mizumoto, D.; Nojiri, C.; Inomata, Y.; Onishi, M.; Waki, M.; Kido, T.; Sugiyama, T.; Senshu, K.; Uchida, K.; Sakai, K.; Akutsu, T. Comparative blood compatibility of polyether vs polycarbonate urethanes by epifluorescent video microscopy. *ASAIO J.* **1997**, *43* (5), M500−M504.
(34) Coury, A. J.; Slaikeu, P. C.; Cahalan, P. T.; Stokes, K. B.; Hobot, C. M. Factors and Interactions Affecting the Performance of Polyurethane Elastomers in Medical Devices. *J. Biomater. Appl.* **1988**, *3* (2), 130−179.
(35) Solís-Correa, R. E.; Vargas-Coronado, R.; Aguilar-Vega, M.; Cauich-Rodríguez, J. V.; Román, J. S.; Marcos, A. Synthesis of HMDI-based segmented polyurethanes and their use in the manufacture of elastomeric composites for cardiovascular applications. *J. Biomater. Sci., Polym. Ed.* **2007**, *18* (5), 561−578.
(36) Shah, N.; Sax, J. E.; Ottino, J. M. Influence of morphology on the transport properties of polystyrene/polybutadiene blends: 2. Modelling results. *Polymer* **1985**, *26* (8), 1239−1246.
(37) Mishra, A.; Aswal, V. K.; Maiti, P. Nanostructure to Microstructure Self-Assembly of Aliphatic Polyurethanes: The Effect on Mechanical Properties. *J. Phys. Chem. B* **2010**, *114* (16), 5292−5300.
(38) Yuliya, B.; Marie, U., Modern Polyurethanes: Overview of Structure Property Relationship. In *Polymers for Personal Care and Cosmetics*; American Chemical Society: 2013; Vol. *1148*, pp 65−81. DOI: doi:10.1021/bk-2013-1148.ch00410.1021/bk-2013-1148.ch004.
(39) Pongkitwitoon, S.; Hernández, R.; Weksler, J.; Padsalgikar, A.; Choi, T.; Runt, J. Temperature dependent microphase mixing of model polyurethanes with different intersegment compatibilities. *Polymer* **2009**, *50* (26), 6305−6311.
(40) Sax, J.; Ottino, J. M. Modeling of transport of small molecules in polymer blends: Application of effective medium theory. *Polym. Eng. Sci.* **1983**, *23* (3), 165−176.
(41) Diederichsen, K. M.; Brow, R. R.; Stoykovich, M. P. Percolating Transport and the Conductive Scaling Relationship in Lamellar Block Copolymers under Confinement. *ACS Nano* **2015**, *9* (3), 2465−2476.
(42) Kirkpatrick, S. Classical Transport in Disordered Media: Scaling and Effective-Medium Theories. *Phys. Rev. Lett.* **1971**, *27* (25), 1722−1725.
(43) Hofmeister, I.; Landfester, K.; Taden, A. Controlled Formation of Polymer Nanocapsules with High Diffusion-Barrier Properties and Prediction of Encapsulation Efficiency. *Angew. Chem., Int. Ed.* **2015**, *54* (1), 327−330.

DOI: 10.1021/acsbiomaterials.6b00215
ACS Biomater. Sci. Eng. 2016, 2, 1483−1492